FLUX AND SALT REJECTION ENHANCEMENT OF POLYVINYL(ALCOHOL) REVERSE OSMOSIS MEMBRANES USING NANO-ZEOLITE

Shaheen Fatima Anis[a], Raed Hashaikeh[a], Nidal Hilal[a, b*]

[a] NYUAD Water Research Center. New York University Abu Dhabi, P.O. Box 129188, Abu Dhabi, United Arab Emirates

[b] Centre for Water Advanced Technologies and Environmental Research (CWATER), College of Engineering, Swansea University, Fabian Way, Swansea SA1 8EN, United Kingdom

[*]Corresponding author

Abstract

Zeolite based membranes have been extensively studied over the past decade for enhanced reverse osmosis (RO) performances. In this study, poly vinyl alcohol (PVA)-networked cellulose (NC) membranes incorporated with nano zeolite-Y were prepared through a facile slip casting approach using various nano zeolite-Y loadings from 0.05 to 1.0 wt. %. The nano zeolite was prepared through a unique ball milling process. Membrane hydrophilicity was seen to increase with increase in zeolite loading, while improved tensile strength (8.7 MPa) and tensile modulus (67MPa) were obtained on small zeolite additions of 0.05wt. %. No prominent peak shifts were observed in differential scanning calorimeter (DSC) testifying to the thermal stability of the membranes.

Membranes were tested for RO using 25,000 mg/L NaCl solution. Optimum RO performance was achieved for 0.5 wt. % nano zeolite registering a salt rejection (R_s) of 99.52% with a flux increase of 34.2 % compared to the bare PVA-NC membranes. Thus, addition of nano-Y to the polymer matrix provides preferential water pathways which facilitates water flow through the membrane. In addition, the irregular crystal morphology of the nano-Y, the size exclusion principle and the ion exchange mechanism provided a high salt rejection for the PVA-NC-nano Y membranes.

Keywords: Polyvinyl alcohol, Networked cellulose, Nano zeolite-Y, Membranes, Reverse osmosis

1. INTRODUCTION

Reverse osmosis (RO) has globally emerged as a promising desalination technology with remarkable advances made in this field during the past few decades [1-3]. With the ever increasing demand for potable water, and increased stress on reduced capital costs, RO membrane materials have always been a topic of experimental and computational research [4, 5]. Continuous improvement is sought in water flux, salt rejection and membrane fouling resistance where improving one property may adversely affect the other [6]. These improvements largely focus on improved, novel membrane materials and modifications to the existing ones [7, 8]. Among several RO polymeric membrane materials, polyvinyl alcohol (PVA), owing to its inherent hydrophilicity [9] and excellent film forming [10] ability has long been studied for this application. Anis et al. [11] reported a study on PVA-networked cellulose (NC) membranes and corresponding membrane characteristics for RO performance. NC was used to control PVA's swelling in water. A flux of 1.435 l/h·m^2 was reported with a salt rejection of 98.9 % for a PVA-NC membrane with ~200µm thickness for a 25000mg/L feed. The PVA-NC membranes with 20 wt. % NC registered superior mechanical properties with a Young's Modulus of 1670MPa and 2.9MPa for dry and wet states respectively.

The emergence of nanomaterials as functional materials [12-14] has led to their use in membrane modification [15-17]. Zeolites represent one such class of material which has gained interest for RO membranes [18, 19]. Zeolites are crystalline aluminosilicates which possess an ordered inorganic structure [20, 21]. Its network of channels and micropores act as molecular sieves providing size-selectivity for salt ions, which render the material attractive for desalination applications [22]. Faujisite (FAU) type zeolites such as zeolite-X and zeolite-Y are reported to be favorable candidates for seawater desalination applications [23] where their pores have diameters smaller than the

hydrated salt ions [4]. Zeolite-Y consists of sodalite cages and their inter-crystalline pores form a 3-D channel system by a 12-membered ring, having a diameter of 7.4A^{o} which form preferential water pathways [24]. Zeolites with a high Al_2O_3 content (low Si/Al ratio) usually have more defects in the form of grain boundaries, and hence are reported for reduced selectivity [25, 26].

RO membranes utilizing inorganic materials is a novel application as limited work has been reported in this field of study compared to organic membranes which are already commercialized and possess a strong hold in the desalination market today [3]. Therefore, extensive research is required to improve the performance of such inorganic based membranes, whereby membrane characteristics can be altered by incorporating different inorganic fillers into a polymeric matrix. Theoretical calculations show that zeolite based membranes are capable of completely excluding hydrated ions due to their well-ordered pore structure [3]. Various approaches may be adopted for utilizing zeolites in membranes including embedment of zeolite nanoparticles in a polymeric matrix [27], coating or hydrothermal growth of zeolite layer on a porous support [28] and self-supported zeolite films [29]. Kazemimoghadam [18] reported thin, active layer of Hydroxysodalite (HS) zeolite grown hydrothermally on a porous mullite support which gave a flux of 4 L/m^{2}h. Li et al. [22] synthesized alumina supported MFI-type zeolite membranes through in-situ crystallization. A 76.7% rejection of Na^+ was achieved with a water flux of about 0.112 kgm^{-2}.h^{-1} for 0.1M NaCl feed. Fathizadeh et al. [30] synthesized NaX zeolite/polyamide (PA) membranes for RO where they achieved a flux which was 1.8 times higher compared to the neat PA membrane with no change in salt rejection. Lind, al. [31] reported high water fluxes for LTA/PA TFC RO membranes, however with a detrimental effect on the salt rejection. Zeolite-Y was reported to be used by Dong et al. [24]. They fabricated RO

membranes embedded with zeolite-Y nanoparticles via interfacial polymerization (IP) of trimesoyl chloride (TMC) and m-phenylenediamine (MPD) on nanoporous polysulfone (PSf) supports. Zeolite-Y nanoparticles were prepared through hydrothermal synthesis, where its particle sizes ranged from 100-200nm with a Si/Al ratio of 1.7. Water flux was reported to increase from 0.95 to 1.92 m^3/m^2/day with zeolite incorporation, together with a slight increase in salt rejection (98.8% from 98.5%) for brackish water. In general, zeolite modified membranes are reported to show superior thermal and chemical stability, along with improved RO performances in contrast to membranes without zeolite addition [32].

In this study, we have studied the RO performance by varying the concentration of HY nano zeolite in the PVA-NC matrix. HY was produced through the ball milling approach [33]. The ball milling of micron sized zeolite-Y enabled the production of nano zeolite-Y with high Si/Al ratios with its nominal cation form of hydrogen. RO performance of nano zeolite-Y was compared with the commercially available Linde type L zeolite, nano-LTL for high saline feed water using similar test conditions. Zeolite based membranes offer exciting performance upgrades and thus this study will provide further insight on utilizing these crystalline aluminosilicates for RO application.

2. EXPERIMENTAL

2.1 Materials

Microcrystalline cellulose (MCC) was purchased from FMC Biopolymer (Philadelphia, PA). Zeolite-Y (CBV 720) was purchased from Zeolyst International while nano zeolite-LTL (Lucidot NZL 40 LP 3533) was purchased from Clariant. Carbon nanostructures (CNS) were purchased from Applied Nanostructured solutions LLC. PVA (Mw = 145,000 and 99.0–99.8 mol. % hydrolyzed), ethanol and sulfuric acid (99.99%) were purchased from Sigma Aldrich (St. Louis, MO). Sulfuric acid was diluted to 70% (w/w) concentration for cellulose modification.

MCC was modified via acid hydrolysis through a procedure reported in [34], using a Varian® dissolution system. During acid addition, the bath temperature was maintained at 5°C. 5 g of MCC was slowly added to 50ml of sulfuric acid and the resulting solution was stirred at 250 rpm for 30 min at 5°C, until a viscous, transparent liquid was obtained. After 30 min, ethanol was added to the viscous solution in order to regenerate the cellulose. The resulting mixture was allowed to stir for further 10 min. Centrifugation of the mixture was performed at 2400 rpm at 4 °C in order to decant the acidic layer. The centrifugation process was repeated around three times for acid removal, after which the suspension was put into a dialysis membrane using a Spectra/Por (MWCO: 12–14,000) dialysis membrane. Dialysis under running tap water was continued until the pH of the suspension reached about neutral. After dialysis, the NC precipitate was sonicated and mechanically homogenized using a Hielscher Ultrasonic Processor UP400S and IKA-T25 ULTRA-TURRAX respectively.

Nano zeolite-Y was produced through the ball milling method as reported in [33]. In brief, ball milling of micron sized zeolite was carried out using E-max high energy ball mill machine (Retsch, Germany) using zirconia jars with 2mm zirconia balls. Zeolite: CNS weight ratio was kept as 3: 1, while the water: ethanol ratio was kept as 1: 1 by volume. Ball milling was carried out at 1000 rpm for 1 hour. After

ball milling, the samples were centrifuged at 4000 rpm for 10 min in a centrifuge machine (Thermo Scientific, Heraruss Megafuge 40R centrifuge) to separate the nano-Y from the solvent. After separation of the particles, the samples were dried in an oven at 80 °C overnight. CNS was thereafter removed by oxidation of the samples at 610°C for 5 h using a Nabertherm P330 furnace.

2.2 Preparation of PVA-NC-Nano Zeolite Membranes

A PVA of 5 wt. % was used for fabricating PVA-NC-zeolite membranes. A 20 wt. % NC concentration in PVA solution was chosen according to the study in [11]. PVA-NC solution was mixed with different nano zeolite concentrations of 0.05, 0.1, 0.2, 0.5 and 1.0 wt. %. The suspension was ultasonicated for 30 min prior to casting for a uniform zeolite distribution within the PVA-NC solution. Fixed amounts of PVA-NC–nano zeolite solutions were allowed to cast on a glass plate. The glass plates were left to completely dry at an ambient temperature with the nano zeolite embedded inside the polymer matrix. After drying, the membranes were wetted and freeze dried using a wizard 2.0 by VIRTIS freeze drier system. Membrane thicknesses ranged from 80-100µm. For convenience, the membranes are abbreviated as PVA-NC-Y (0.05), PVA-NC-Y (0.1), PVA-NC-Y (0.2), PVA-NC-Y (0.5) and PVA-NC-Y (1.0) where the letter 'Y' represents nano zeolite-Y. Commercial nano zeolite-L was also tested as a reference material for its performance using a similar approach. The samples were labelled as PVA-NC-L (0.05), PVA-NC-L (0.1), PVA-NC-L (0.2), PVA-NC-L (0.5) and PVA-NC-L (1.0), where 'L' represents nano-LTL zeolite and the numbers in the bracket represent the wt. % of nano-LTL in the PVA-NC solution.

Figure 1: (a) PVA-NC-nano zeolite-Y solution being cast and dried on a glass slide (b) PVA-NC-nano zeolite-Y membranes after drying and peeled off from the glass slide.

2.3 Membrane characterization

Structural integrity of the membranes was studied through X-ray diffraction (XRD, Panalytical Empyrean diffractometer) at 40 kV and 30 mA, with Ni-filtered CuKα (λ = 1.5056 Å) radiations in 5–70° half angle range. Full width at half maximum (FWHM) was calculated to study the change in crystallinity of the membranes if any. Membrane structure was viewed using transmission electron microscope (TEM, talos F200X, FEI). Images were taken in the bright field mode. TEM sample was prepared by solution drop cast method whereby a small droplet (<1 µl) of PVA-NC-Y (0.5) was dropped on a carbon coated copper grid. Membrane morphology was viewed using scanning electron microscopy (SEM, FEI Quanta 450), operating at 10 kV. The samples were coated under vacuum with gold (≈5nm) prior to SEM analysis. Energy dispersive spectroscopy (EDS), (EDAX) was used in conjunction with SEM to study the membrane's elemental composition qualitatively. Atomic force microscopy (AFM, Alpha 300 Witec) was used to study the surface roughness of the PVA-NC-Y membranes. Related parameters (including R_t and R_{tm}) were determined through the AFM analysis

software (Gwyddion). R_t is the maximum height of roughness while R_{tm} gives the average maximum height of the membrane roughness. Attenuated total reflectance infra-red (ATR-IR, Cary 600 Series, Agilent Technologies) Fourier transform infra-red (FTIR) spectrometer) was used to determine the functional groups on the membrane's surface. Membrane samples were dried in a vacuum oven at 30°C prior to ATR-IR measurements. Thermal characteristics of the membranes such as thermal degradation behavior and melting peaks were studied through thermo-gravimetric analysis (TGA) and differential scanning calorimeter (DSC) respectively using a SDT Q600. Samples (≈10mg) were placed in a sample pan and heated from room temperature to 1000°C at a rate of 10 °C/min with a nitrogen flow of 20 ml/min. Tensile strength and tensile modulus of the membranes were studied in both dry and wet state, using Instron, model No. 5982. A load cell of 5 kN at a strain rate of 1 mm/min were used for this purpose. Membrane wettability was determined through contact angle instrument (OCA 15EC). A sessile drop approach was used. 2 µL droplet of deionized (DI) water was used as the testing liquid and contact angle was evaluated by tangent and circle methods using the SCA software.

2.4 Reverse Osmosis Test

RO testing on the membranes was performed using an in-lab RO unit, similar to the one reported in [11]. A feed concentration of 25,000 mg/L NaCl was used. Before testing, membranes (diameter 41.8cm) were wetted and freeze dried using a wizard 2.0 *VIRTIS* freeze drier system. They were then allowed on a polysulfone (PSf) UF membrane support provided by LENNTECH, GE Osmonics. Figure 2 depicts the schematic of the membrane and the support used.

Testing time was 30 min under a pressure of 25 bars. Flux (J) was measured by dividing the volume of permeate collected by the area of the membrane and the testing time. The permeate collected was measured for its conductivity using an accumet® XL 50 dual channel pH/Ion/Conductivity meter. The selectivity (Rs) was calculated using the conductivity differences between the feed solution and the permeate solution:

$$\%\ \boldsymbol{salt\ rejection} = \frac{\boldsymbol{feed\ conductivity}\left(\frac{S}{cm}\right) - \boldsymbol{permeate\ conductivity}\left(\frac{S}{cm}\right)}{\boldsymbol{feed\ conductivity}\left(\frac{S}{cm}\right)} \times \mathbf{100}$$ Equation 1

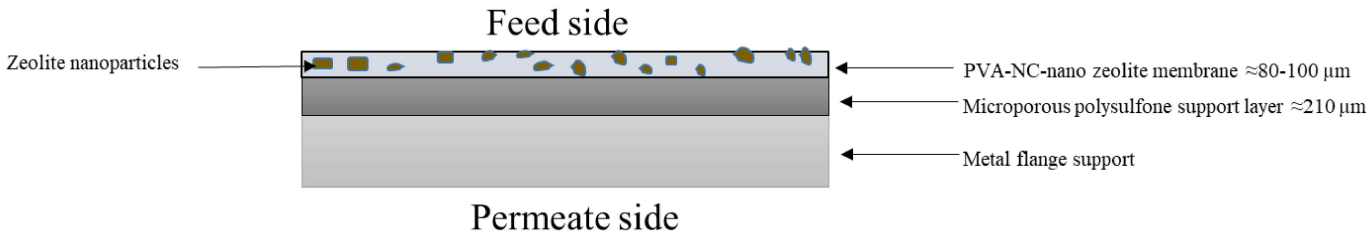

Figure 2: Schematic of the PVA-NC membrane supported by PSf and the metal flange

3 RESULTS AND DISCUSSION

3.4 Structural Stability

X-ray diffractograms for PVA-NC, PVA-NC-Y (0.05), PVA-NC-Y (0.1), PVA-NC-Y (0.2), PVA-NC-Y (0.5) and PVA-NC-Y (1.0) are shown in Figure 3a, while Figure 3b shows the XRD pattern for pure nano zeolite-Y particles. With low zeolite concentrations below 0.5 wt. %, no zeolite peaks were detected. Similar has been reported in [35, 36] where no XRD peaks were registered for phases with low concentrations. With an increase in zeolite addition, all major peaks for nano zeolite-Y, $2\theta<20^{o}$ were detected as highlighted in Figure 3a. Figure 3c shows the XRD patterns for PVA-NC incorporated with nano zeolite-LTL, while Figure 3d shows the XRD pattern of pure nano LTL particles. Again, peaks from nano-LTL were detected in only two samples, PVA-NC-L (0.5) and PVA-NC-L (1.0), while lower concentrations did not register any major zeolite-L peaks. Figures 3d and 3e show the change in full width at half maximum (FWHM) with increasing zeolite wt.% in the samples. With nano zeolite-Y, an increase in FWHM values is observed indicating peak broadening and hence a decrease in crystallinity of the composite membrane. This can in turn increase the performance of RO membranes as amorphous regions let the water to pass through it while the crystalline region does not [11]. The reason for membrane's increased amorphousness may be attributed to the fact that nano zeolite-Y was produced through the ball milling approach which rendered it with reduced crystallinity compared to the parent micro zeolite-Y particles as discussed in [33]. Nevertheless, with nano zeolite-LTL, the FWHM is almost similar for all zeolite wt.% except for PVA-NC-L (0.05), which showed an increase in FWHM with 3.2 degrees from 3.0 degrees.

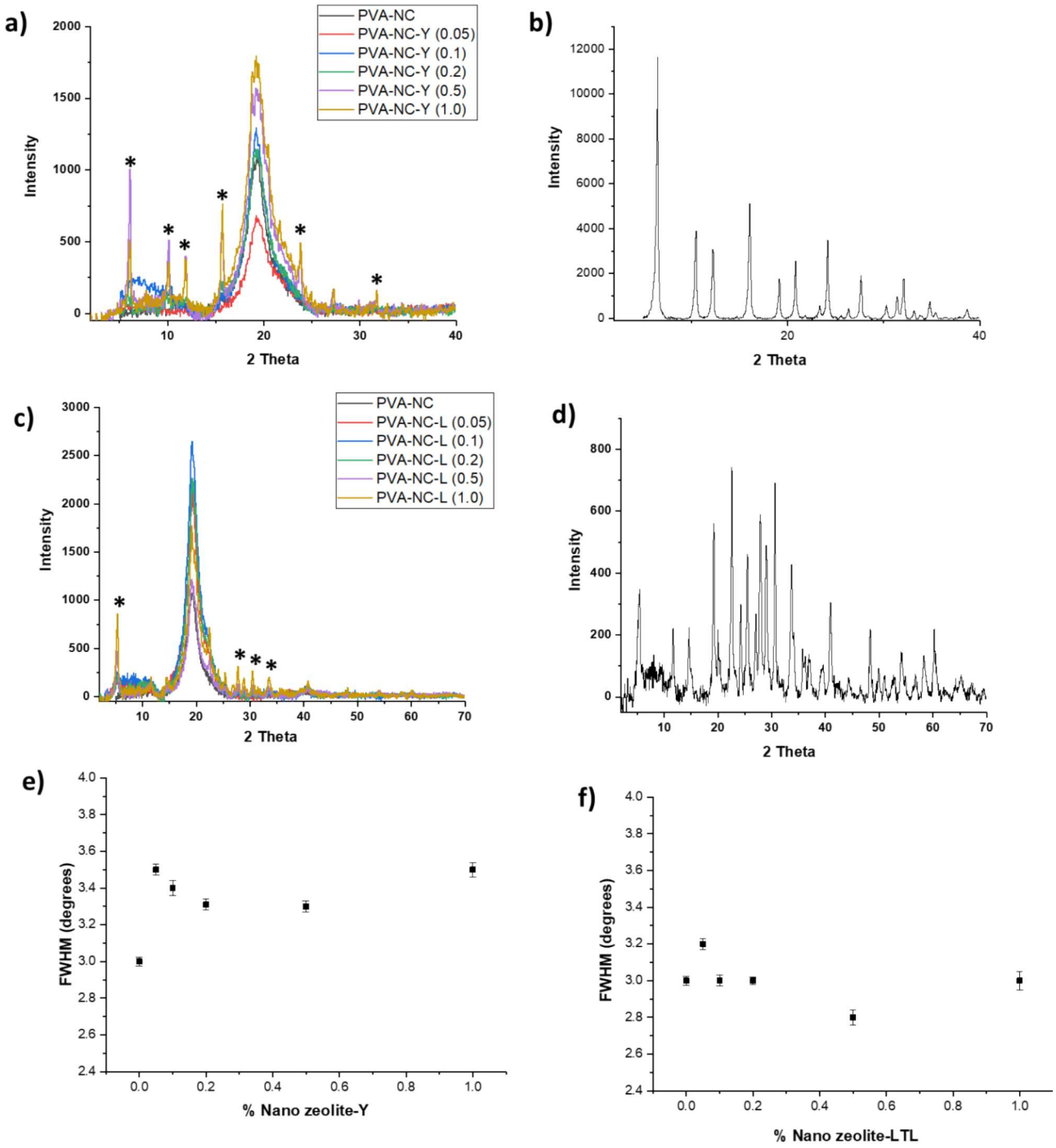

Figure 3: XRD patterns for (a) PVA-NC-Y (b) Nano zeolite-Y particles (c) PVA-NC-L (d) Nano zeolite-LTL particles; variation in FWHM with increasing zeolite wt.% for (e) Nano zeolite-Y (f) Nano zeolite-LTL

Figure 4a compares the DSC curves for PVA-NC and PVA-NC-Y membranes. The first endothermic peak centering at 115°C is due to moisture evaporation owing to PVA's [11] and zeolite's [37] hydrophilic nature. Melting peaks were observed at 229°C (as highlighted with the dashed line in Figure 4a) which agrees with the existing literature [11]. No prominent peak shifts were observed testifying to the thermal stability of the membranes. PVA degradation peak was observed around 350°C. Figure 4b shows the TGA curves for PVA-NC and PVA-NC-Y membranes. The loss in weight during room temperature to 200°C is attributed to the evaporation of residual water. PVA decomposition takes place above 230°C while zeolites are thermally stable up to high temperatures above 1000°C. Thermal analysis of the membranes do not show any prominent variation in thermal properties for PVA-NC membranes previously reported [11].

.

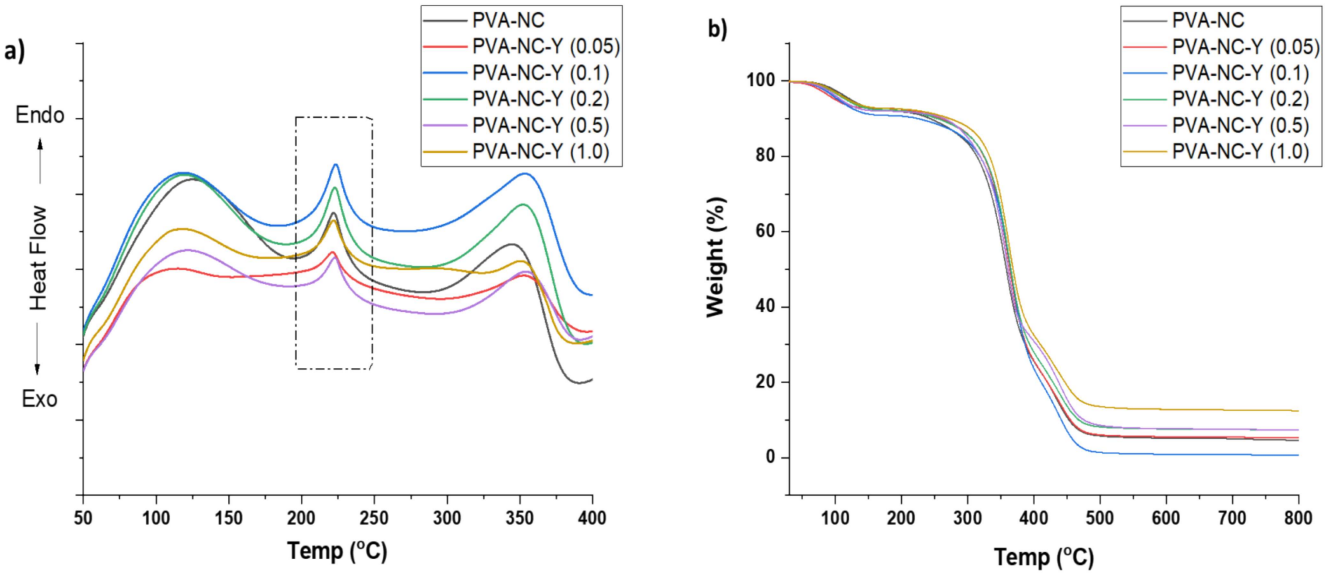

Figure 4: (a) DSC curves showing the melting and decomposition temperatures for PVA–NC-Y membranes (b) TGA curves showing the degradation profile for PVA–NC-Y membranes

Figure 5a shows the ATR-IR spectra from 4000 to 500cm^{-1} of the PVA-NC and PVA-NC-Y (1.0) membranes. ATR-IR spectroscopy can provide an insight on the chemical bonds present in the sample. No obvious difference was spotted between the two spectra, with the major bands of O-H, C-H, C-C and C-O observed in both the cases. The large bands observed between 3500 to 3100 cm^{-1} are due to the O-H stretching from the intermolecular and intramolecular hydrogen bonds in the PVA polymer. The vibration band in the 3000 - 2800 cm^{-1} range represents the C-H stretching from the alkyl group. The stretching C=O and C-O bonds are from the acetate groups remaining from PVA. The characteristic zeolite peaks from Si-O and Al-O in the range of 1100-950 cm^{-1} (Figure 5b) could not be revealed explicitly due to the relatively low zeolite loading and the possibility of being covered by the strong C-O stretching peak [38, 39] in the same wavelength range. Nevertheless, zeolite presence was confirmed through XRD as discussed before and through SEM-EDS as discussed in section 3.2.

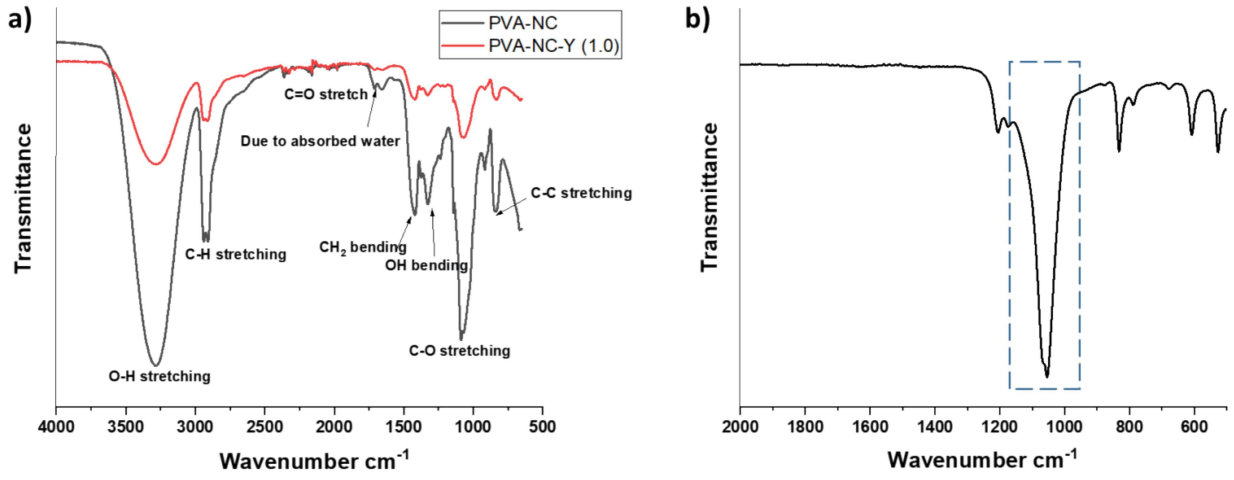

Figure 5: ATR-IR spectra of (a) PVA-NC and PVA-NC-Y (1.0) membranes from 4000 to 500 cm^{-1} (b) zeolite-Y from 2000 to 500cm^{-1}, the dotted box highlights the characteristic peak for zeolites around 1100cm^{-1}.

3.5 Membrane Morphology

Figures 6a and 6b show TEM images of nano zeolite-Y and nano zeolite-LTL particles respectively. The particle sizes for both zeolites were <100nm. Figure 6c shows the TEM image of PVA-NC where the networked structure of NC can be seen entrapping the PVA polymer inside its network. This does not let the PVA to expand or swell when in contact with water. Figure 6d shows the TEM image of PVA-NC with the addition of nano-zeolite Y particles. The nano zeolite-Y particles (some of which are highlighted by the blue arrow) can be seen to be distributed uniformly within the PVA-NC network. Figures 7(a-f) show SEM images of all the fabricated PVA-NC membranes with nano zeolite-Y. With increasing percentage of nano zeolite from 0.05 wt. % to 1.0 wt. % in PVA-NC, the zeolite particles can be detected more readily on the membrane's surface. Figure 7b does not show any zeolite nanoparticles on the membrane's while at higher zeolite wt.% such as in Figure 7f, the particles can be seen to be agglomerated. Agglomeration of nanoparticles [40] is a common problem whereby owing to the high surface energy of the particles, they tend to cluster. The presence of zeolite particles was also confirmed through EDS analysis as shown in Figure 8. Figures 8(a-b) show SEM images and their corresponding EDS spectrum for the EDS spots highlighted in the SEM image. Various elemental signals were detected including Al, Si and O due to nano zeolite-Y, C and O due to the polymer matrix and Au due to the coating on the sample. It is interesting to note the high Si peak detected compared to Al, apparently because the zeolite-Y used in this study is a high Si/Al ratio zeolite.

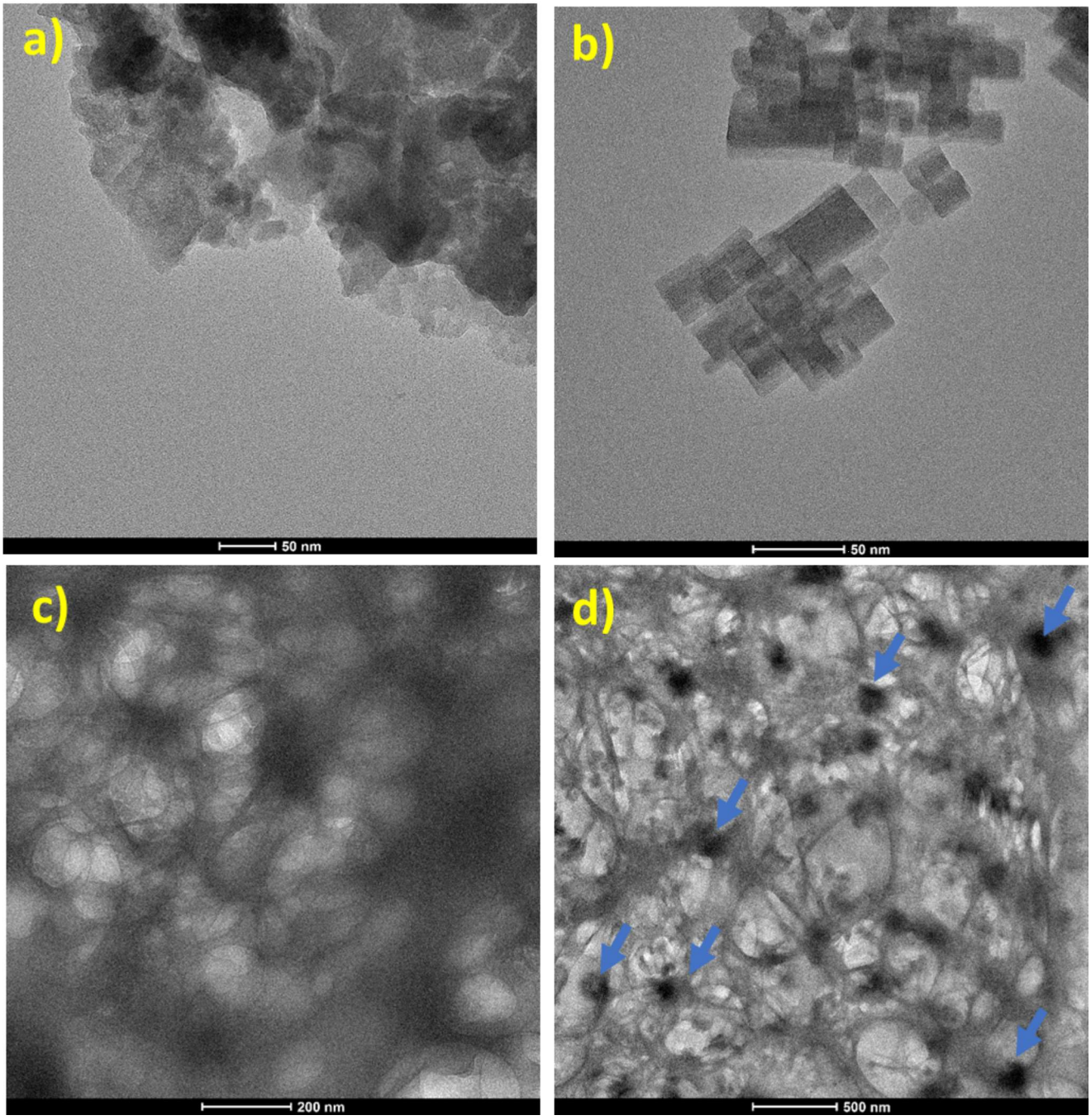

Figure 6: TEM images of (a) Nano zeolite-Y (b) Nano zeolite-LTL (c) PVA-NC (d) PVA-NC-Y(0.5). The blue arrows highlight the zeolite particles.

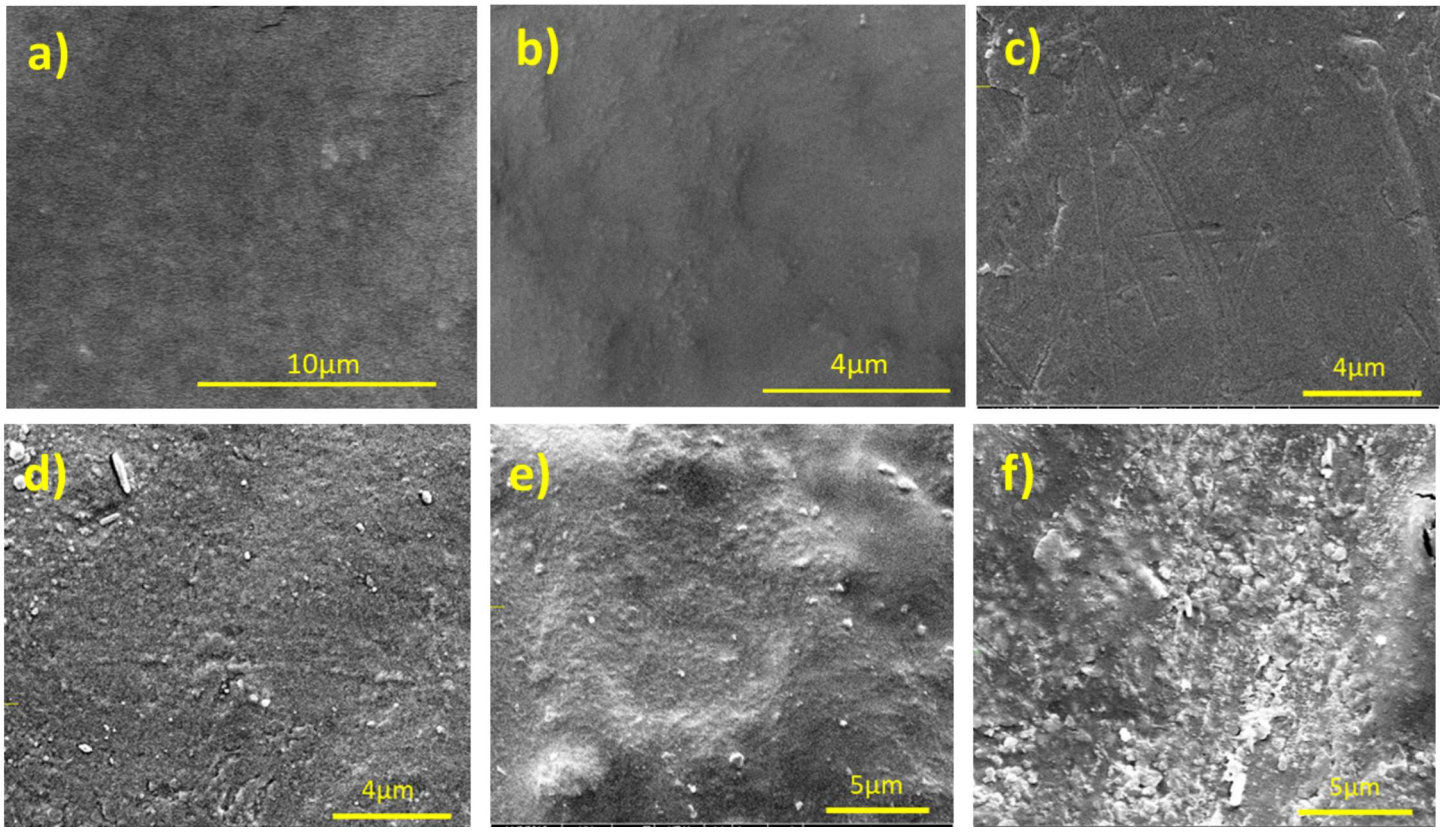

Figure 7: SEM images of (a) PVA-NC (b) PVA-NC-Y (0.05) (c) PVA-NC-Y (0.1) (d) PVA-NC-Y (0.2) (e) PVA-NC-Y (0.5) (f) PVA-NC-Y (1.0)

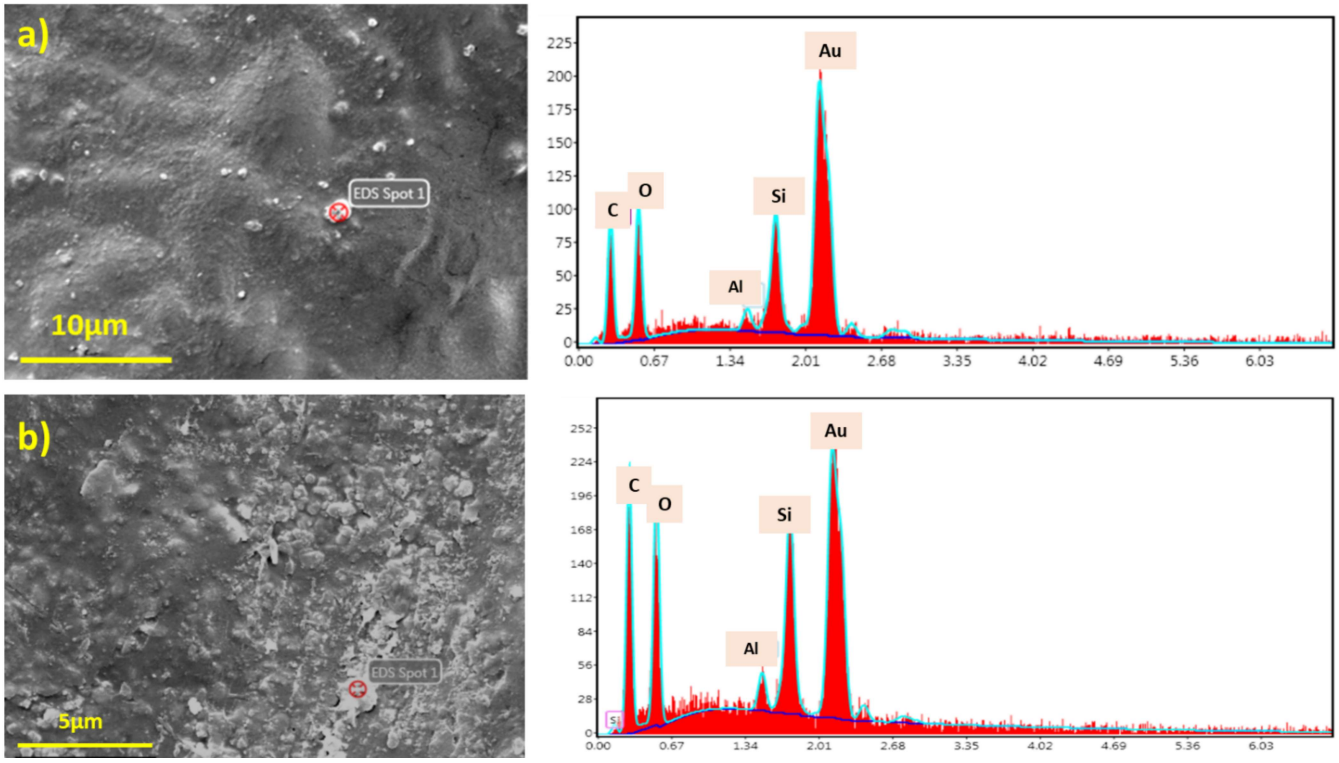

Figure 8: (a) SEM image of PVA-NC-Y (0.5) and the corresponding EDS spectrum for the EDS spot 1 highlighted in the SEM image (b) SEM image of PVA-NC-Y (1.0) and the corresponding EDS spectrum for the EDS spot 1 highlighted in the SEM image

Figure 9a shows the surface morphology of PVA-NC-Y (0.5) membrane as revealed by the AFM image while imaging in the non-contact mode. The surface roughness of the nano-Y embedded membranes was measured from the AFM image as shown in Figure 9b. Three lines were chosen (not shown in the image) to study the roughness profile of the membranes. The R_t values as calculated by the software were 60.27nm, 45.56nm and 48.68nm while the R_{tm} values were 37.95nm, 25.70nm and 30nm. These small values attest to the smoothness of the membrane's surface and hence minimal agglomeration of the zeolite nanoparticles in the PVA-NC matrix which does not lead to a highly rough surface and is well in comparison to the neat PVA-NC membranes reported previously [11].

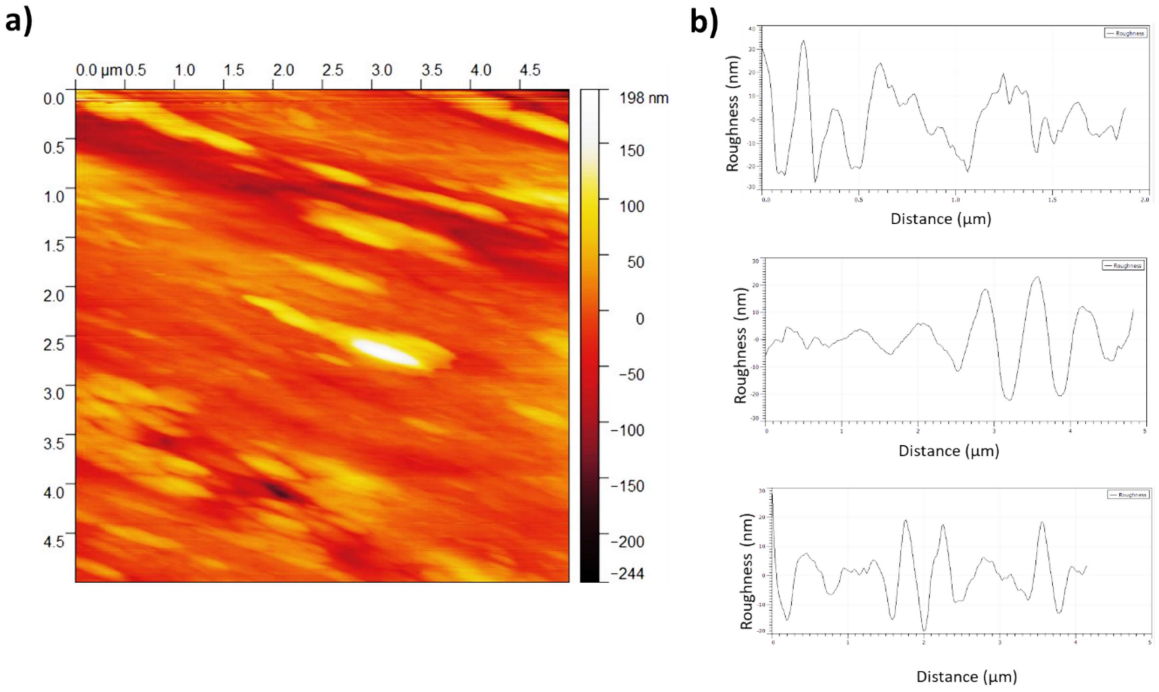

Figure 9: (a) PVA-NC-Y membrane morphology as revealed by AFM (b) Surface roughness profile over three random lines on the AFM image.

3.6 Membrane Wettability

Figure 10 shows the variation in membrane hydrophilicity with increasing nano-Y loading in PVA-NC membranes. The PVA-NC membrane showed a low contact angle of 28.8^{o}±0.3. This is due to PVA's hydrophilic nature and thus a high affinity for water. A decrease in contact angle was registered with progressive zeolite addition. The hydrophobicity of FAU zeolites decreases with an increase in Si/Al ratio [41]. Hence, with a high Si/Al ratio of 30, an increase in hydrophilic functionality in apparent. Thus, zeolite-Y nanoparticle addition increases the affinity for water and hence decreases the contact angle at the membrane's surface. Similar decrease in contact angle with zeolite addition is reported in [24, 30]. In general, surface wettability increases with increasing surface roughness [42]. The decrease in contact angle, or increased wettability might also be attributed to the increasing roughness of the membranes with progressive zeolite addition as apparent from Figure 7. It is interesting to note the slight increase in the contact angle for PVA-NC-Y (1.0). This might be due to nanoparticle aggregation. As discussed in section 3.2, for higher zeolite loading beyond 0.5 wt.%, zeolite nanoparticles were seen to be agglomerated on the membrane's surface. This can lead to a reduction in active surface area of the nanoparticles and their influence on membrane hydrophilicity. Similar observation is reported in [27]. Membrane's hydrophilicity and morphology are important factors for controlling membrane permeability and selectivity.

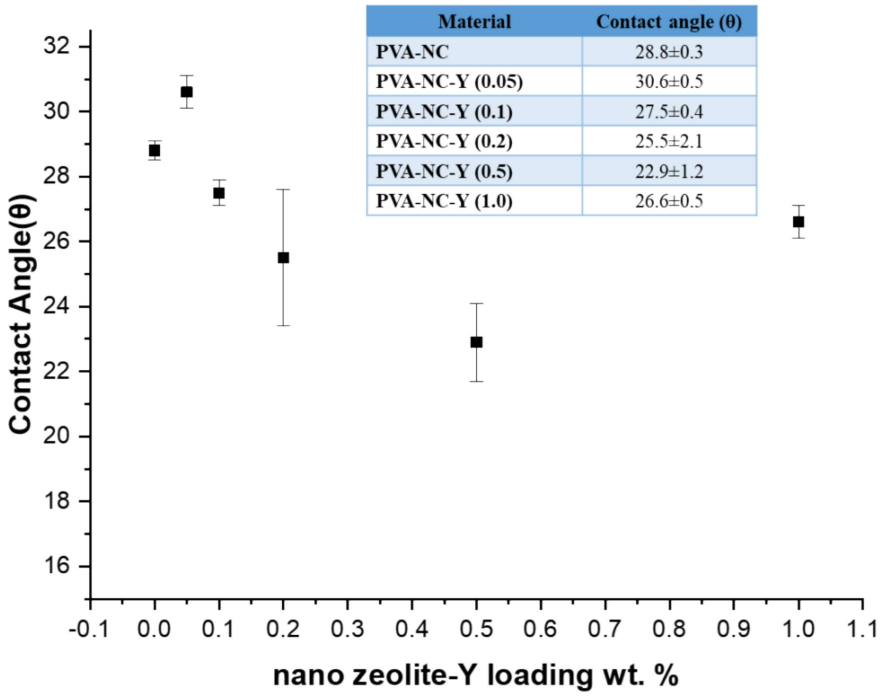

Figure 10: Effects of nano zeolite-Y loading on pure water contact angles of PVA-NC-Y membranes

3.7 Mechanical Properties

Table 1 summarizes the mechanical properties of PVA–NC-Y membranes. Tensile properties were studied both in dry and wet specimen states. Figures 11a and 11b show the stress-strain graphs for dry and wet membranes respectively. The results for both are quite different, with the dry state registering higher tensile strengths and greater tensile modulus compared to the wet state. This is due to the weakening of the PVA polymeric chains on moisture absorption. Similar is reported in [11]. Besides PVA, zeolite is also hydrophilic and hence absorbs moisture (as discussed in section 3.3). Thus, a lower tensile strength is expected for PVA-NC membranes with zeolite addition. This is

apparent with the tensile strength of dry PVA-NC-Y membrane being dropped from 20.3 MPa for PVA-NC to 14.5 MPa for PVA-NC-Y (1.0).

It is interesting to note a slight increase in the tensile strength of PVA-NC-Y membranes with zeolite addition in the wet condition. Figure 11b shows that the stress-strain graphs reflect the stretchy behavior of the material in the wet state. The zeolite nanoparticles act as a reinforcing agent, whereby increasing both the strength and modulus. This initial improvement in the mechanical properties is most probably due to the strong interfacial bonding between the PVA and zeolite nanoparticles. However, with greater percentages beyond 0.1 wt. %, the strength and modulus decreased with the lowest registered for PVA-NC-Y (1.0). This decrease in strength is also reported in [27], and is attributed to the formation of nanoparticle agglomerates and clusters into the membrane structure. In both the dry and wet states, a small nano zeolite-Y loading percentage ≈ 0.05 wt. % was sufficient to increase the tensile modulus of the membranes. Thus, improved mechanical properties were obtained with a small zeolite addition. However, these small loadings were not sufficient to obtain enhanced RO performance parameters as discussed in section 3.8.

Table 1: Mechanical behavior of PVA–NC-Z membranes.

Material	Dry state		Wet state	
	Tensile strength (MPa)	Tensile modulus (MPa)	Tensile strength (MPa)	Tensile modulus (MPa)
PVA-NC	20.3	503	4.5	42
PVA-NC-Y (0.05)	17.9	900	8.7	67
PVA-NC-Y (0.1)	15.6	690	8.1	49
PVA-NC-Y (0.2)	14.0	568	6.4	34
PVA-NC-Y (0.5)	15.6	581	5.6	28
PVA-NC-Y (1.0)	14.5	236	2.4	19

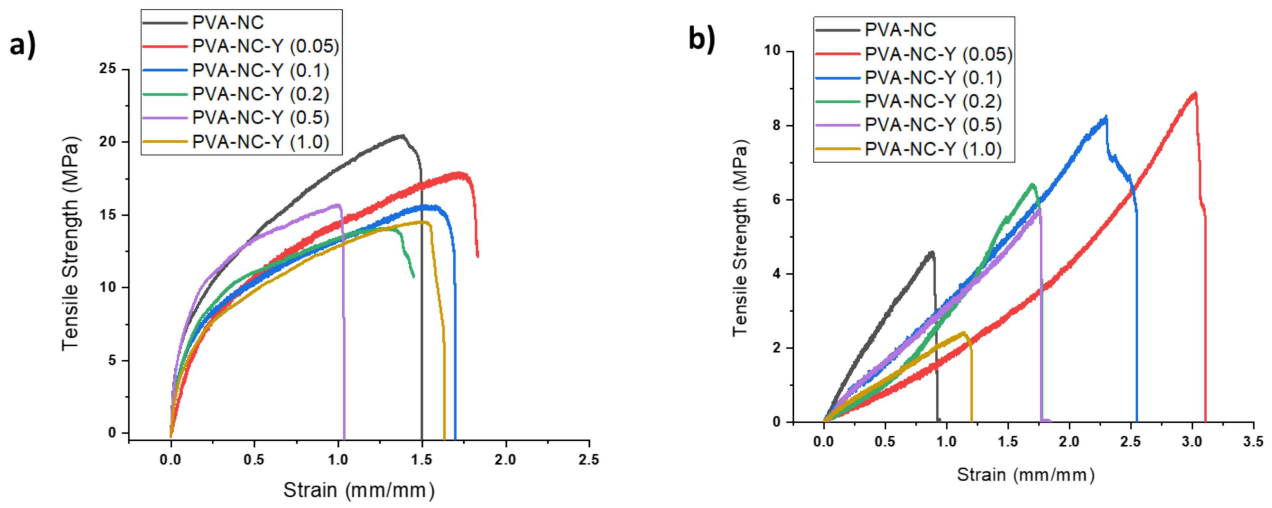

Figure 11: Stress vs. strain graphs for PVA-NC-Y membranes in (a) dry and (b) wet states

3.8 Effects of nano Zeolite Loading on RO Performance

Flux and salt rejections for PVA-NC-Y membranes for a 25000 mg/L NaCl feed solution are tabulated in Table 2. A salt rejection of about 98.9% was obtained with PVA-NC membranes, similar to the one reported in [11], under similar testing conditions of pressure and salt concentration. An increase in Rs to 99.92% from 98.90% was observed with a small nano-Y addition of 0.05 wt. % and 0.1 wt. %. A contemporaneous increase in flux was observed till 0.1 wt. % nano-Y loading. The Rs started to slightly decline after 0.1 wt. %, however it was still greater than the bare PVA-NC membranes. PVA-NC-Y (0.5) registered the highest flux of 5.1 l/h·m^2 with a Rs of 99.52%. FAU zeolite (Figure 12a) has a 3-D channel structure which means the channels intersect with each other providing a high water permeability. The internal porosity of zeolite molecular sieves forms preferential pathways through which the water molecules can easily flow through providing higher water permeation. A high salt

rejection of 99.92% may be attributed to two mechanisms occurring simultaneously; size exclusion and ion exchange in zeolites. The size exclusion principle restricts the passage of sodium ions through the zeolite pores. The Na+ ions exist in the form of stable ionic clusters, tightly bound with the water molecules. These hydrated ions, being larger in size than the zeolite pores (0.8–1.0 nm for $[Na(H_2O)_x]^+$) [22] do not pass through the pores (Figure 12a) which have a diameter of 0.74nm. However, the nanopore channels lead to a smooth water pathway, with no restrictions on the water molecules to pass through the pore channels (Figure 12b). In Figure 12c, the nano zeolite is depicted to be uniformly distributed within the PVA-NC matrix. The top schematic in Figure 12c depicts membranes with low wt. % zeolites which make good contact with the polymer matrix. This does not produce void defects, thus increasing the membrane performance. However, the performance of zeolite nanoparticles decreases when certain parts of the particles are not in contact with the polymer matrix such as those highlighted by a red circle in the same schematic. For these nanoparticles, the interaction is only on the top surface of the membrane. With a high zeolite content, the particles might agglomerate as depicted in Figure 12c bottom schematic. This defect leads to formation of voids and causes low separation efficiency as was observed with PVA-NC-Y (1.0). The lowest Rs of 98.06% was registered by PVA-NC-Y (1.0) with the lowest flux of 2.7 l/h·m^2. Figures 13a-b shows the variation in Rs and J for PVA-NC-Y membranes with increasing nano-Y loading. In general, a gradual increasing trend in Rs and J is observed with increasing nano-Y loading. As discussed in section 3.6, the water contact angle decreased with increasing zeolite loading and the lowest was registered by PVA-NC-Y (0.5). This led to enhanced water permeability. PVA-NC-Y (1.0) gave a contact angle of 27^o, however leading to a lower flux due to nanoparticle agglomeration (Figure 7f), which in turn led to a low membrane performance. Therefore, both membrane

wettability and nanoparticle distribution play a part in RO performance. Secondly, the nano zeolite used in the present study is HY zeolite, in which each aluminium is associated with an H^+ ion. Thus, besides restricting the passage of hydrated Na^+ ions through size exclusion principle, the Na^+ ions will be restricted to diffuse through the zeolite channels by ion exchange on the feed side. It is most probable that the H^+ ions will get exchanged by Na+ as depicted in Figure 12d. Moreover, owing to the high surface area of nano-Y [33], the accessibility to the number of active sites for ion exchange increases which further helps in salt rejection. However, in general, the modified membranes exhibited reduced salt flux, with a simultaneous increase in water flux, indicating enhanced water/salt selectivity at optimum zeolite loadings.

Table 2: RO testing results for PVA-NC-Y and PVA-NC-L membranes at 25 bars. The numbers represent average values of Rs and J.

Material	R_s (%)	J (l/h·m^2)
PVA-NC	98.90	3.8
PVA-NC-Y (0.05)	99.92	4.3
PVA-NC-Y (0.1)	99.92	4.7
PVA-NC-Y (0.2)	99.50	4.1
PVA-NC-Y (0.5)	99.52	5.1
PVA-NC-Y (1.0)	98.06	2.7
PVA-NC-L (0.05)	98.07	4.0
PVA-NC-L (0.1)	97.80	2.0
PVA-NC-L (0.2)	98.80	2.5
PVA-NC-L (0.5)	98.05	2.5
PVA-NC-L (1.0)	97.03	2.5

RO performance of nano-LTL was compared to nano-Y by testing PVA-NC-L membranes using similar testing conditions as for PVA-NC-Y. Table 2 tabulates the Rs and J for PVA-NC-L membranes while

Figure 13c-d shows the same for increasing nano-L loading. Lower permeate fluxes were registered with PVA-NC-L compared to PVA-NC-Y membranes. Zeolite-LTL has a 1D channel system and a low SiO_2/AL_2O_3 (<5) [43]. Molecular diffusion is limited to a single channel as the channels are parallel and do not intersect. This limits the water flow through the zeolite structure. It is interesting to note that the J for PVA-NC and PVA-NC-L (0.05) is quite similar, and a small addition of nano-LTL does not bring about any major change in water flux unlike with PVA-NC-Y membranes. Low rejections of about 98% were registered while the lowest (97.03%) being registered by PVA-NC-L (1.0). This might be due to nanoparticle agglomeration, similar to PVA-NC-Y (1.0). The PVA-NC-L membranes registered lower Rs compared to PVA-NC-Y membranes owing to the high Al_2O_3 content which causes more defects and hence reduced selectivity [25]. Secondly, the low Rs might also be attributed to the well-ordered crystals of the nano-LTL (Figure 12e) which form inter-crystalline pores [22] which may allow the hydrated salt ions to pass through them easily. However, with nano-Y, the zeolite crystals are not well ordered (owing to the ball milling process) and thus, with the random orientation of nano-Y crystals, the probability of inter-crystalline pores decreases as explained in the schematic in Figure 12e and supported by TEM images.

After the test, the membranes showed good mechanical integrity as shown in Figure 14. Figure 14a shows the PVA-NC-Y membrane on a Psf support when placed in the RO cell. Figure 14b shows the same membrane after the test immersed in DI water. It can be seen in Figure 14c that the PVA-NC-Y membrane retained its shape after the test even after removing it from the support layer. This attests to the high pressures the membrane can withstand during the RO operation.

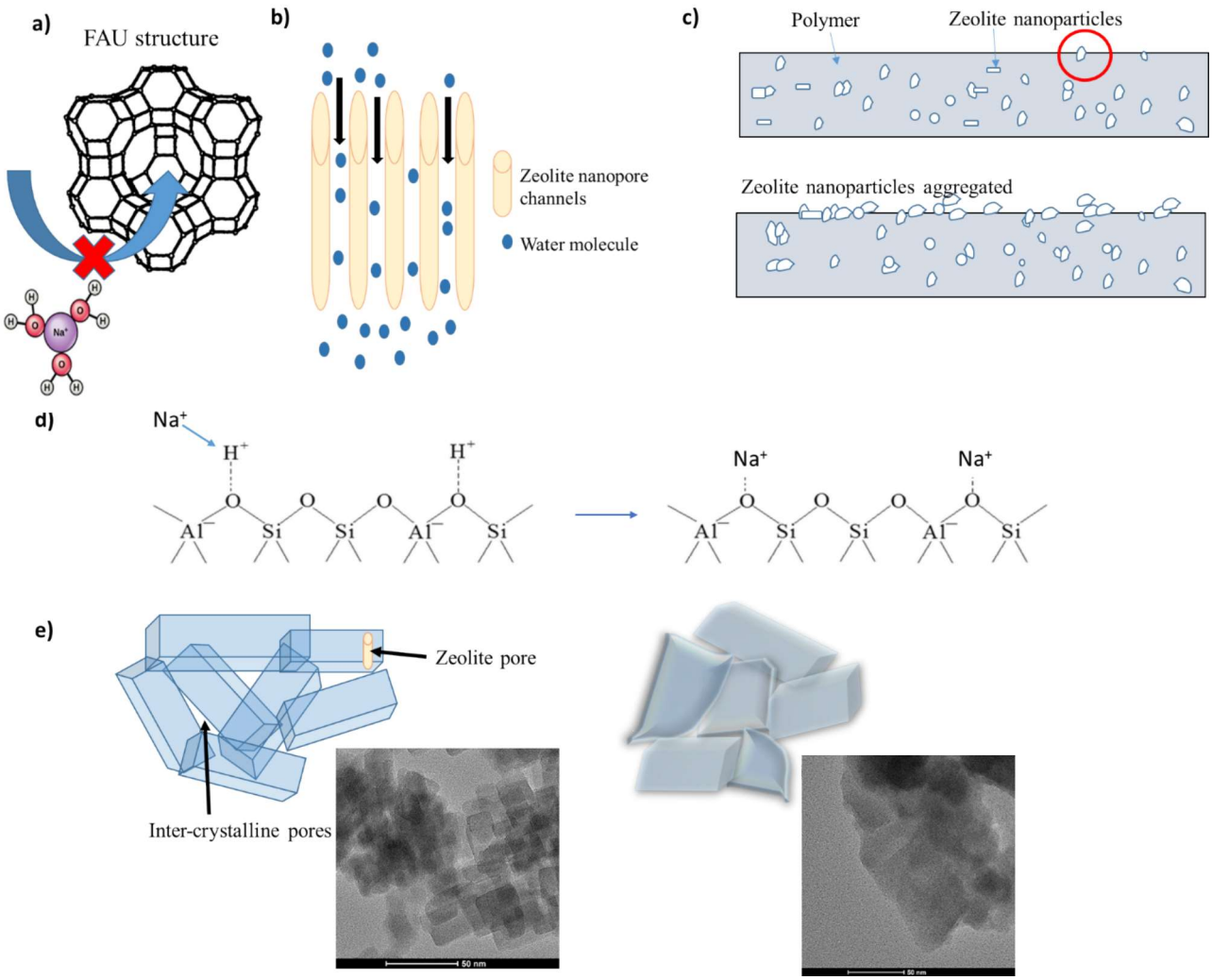

Figure 12: (a) FAU structure with the zeolite nanopores restricting the passage of hydrated salt ions (b) Schematic of nanopore channels facilitating diffusion of water molecules within the zeolite (c) Schematic of PVA-NC-nano zeolite membrane with low (top) and high (bottom) zeolite loadings (d) ion exchange mechanism in the zeolite embedded membranes and (e) Schematic of inter-crystalline pores in well ordered nano-LTL (left) zeolite crystals in contrast to nano-Y (right), supported by TEM images of the two zeolite types.